Molecular Dynamics Simulations of Retinal in Rhodopsin: From the Dark-Adapted State towards Lumirhodopsin†

Vincent Lemaître,‡,§ Philip Yeagle,|| and Anthony Watts*,‡

Biomembrane Structure Unit, Department of Biochemistry, University of Oxford, South Parks Road, Oxford OX1 3QU, United Kingdom, Nestec S.A., BioAnalytical Department, Vers-Chez-Les-Blanc, CH-1000 Lausanne 26, Switzerland, and Department of Molecular and Cell Biology, University of Connecticut, 91 North Eagleville Road, Storrs, Connecticut 06269

Received April 1, 2005; Revised Manuscript Received July 22, 2005

ABSTRACT: The formation of photointermediates and conformational changes observed in the retinal chromophore of bilayer-embedded rhodopsin during the early steps of the protein activation have been studied by molecular dynamics (MD) simulation. In particular, the lysine-bound retinal has been examined, focusing on its conformation in the dark-adapted state (10 ns) and on the early steps after the isomerization of the 11-*cis* bond to *trans* (up to 10 ns). The parametrization for the chromophore is based on a recent quantum study [Sugihara, M., Buss, V., Entel, P., Elstner, M., and Frauenheim, T. (2002) *Biochemistry 41*, 15259−15266] and shows good conformational agreement with recent experimental results. The isomerization, induced by switching the function governing the dihedral angle for the C11═C12 bond, was repeated with several different starting conformations. From the repeated simulations, it is shown that the retinal model exhibits a conserved activation pattern. The conformational changes are sequential and propagate outward from the C11═C12 bond, starting with isomerization of the C11═C12 bond, then a rotation of methyl group C20, and followed by increased fluctuations at the β-ionone ring. The dynamics of these changes suggest that they are linked with photointermediates observed by spectroscopy. The exact moment when these events occur after the isomerization is modulated by the starting conformation, suggesting that retinal isomerizes through multiple pathways that are slightly different. The amplitudes of the structural fluctuations observed for the protein in the dark-adapted state and after isomerization of the retinal are similar, suggesting a subtle mechanism for the transmission of information from the chromophore to the protein.

The rhodopsin-bound retinal is a molecular device for converting light into molecular conformational changes. The irradiation of rhodopsin at 500 nm isomerizes 11-*cis*-retinal to all-*trans*, triggering a chain of conformational changes in the protein that induces signal transduction leading to vision (*1*−*3*). The conformation of retinal and its evolution resulting from light absorption are crucial to an understanding of the activation mechanism of rhodopsin, which has been the subject of intense study (*4*−*6*). Rhodopsin is the most comprehensively studied member of the family of G-protein-coupled receptors (GPCRs)[1] because it is the only GPCR that is naturally present in high abundance in biological tissue (*7*).

Rhodopsin provides an environment in which 11-*cis*-retinal chromophore can undergo a *cis* to *trans* isomerization in response to absorption of a photon with a very high quantum yield of 0.67 (*8*). When light strikes the rod cell and is absorbed by the photopigment, rhodopsin, the resulting structural changes induced by the retinal upon photoactivation produce a series of defined photointermediates (reviewed in refs *3* and *9*). Low-temperature and time-resolved UV/vis spectroscopic measurements have shown that photobleaching of rhodopsin involves several intermediates and may follow more than one pathway (*10*−*12*).

The initial photoproduct, photorhodopsin, is formed within a very short time (200 fs). This state is transient and cannot be isolated (*13*, *14*). A model for the potential energy surface of the excited state based on UV/vis femtospectroscopy data shows that the torsion angle of the bound C11═C12 is changed by 75° within 30 fs, while the full isomerization takes place in 200 fs (*15*). The initial movements of the chromophore are thought to be tightly constrained by the surrounding protein, because of the very short time scale of the photoisomerization (*16*).

† This work was supported by a BBSRC CASE Award to V.L. (Grant number 01/A2/B/07394) and a MRC Programme Grant to A.W. (Grant number G000852).

* To whom correspondence should be addressed. E-mail: anthony.watts@bioch.ox.ac.uk. Telephone: 44-1865 275268. Fax: 44-1865 275234.

‡ University of Oxford.

§ Nestec S.A.

|| University of Connecticut.

[1] Abbreviations: MD, molecular dynamics; GPCR, G-protein-coupled receptor; UV/vis, ultraviolet/visible absorption spectra; NMR, nuclear magnetic resonance; BSI, blue-shifted intermediate; PME, particle-mesh Ewald; SPC, single-point charge; POPC, 1-palmitoyl-2-oleoyl-*sn*-glycerophosphocholine; DFT, Density Function Theory; SMD, steered molecular dynamics; TM, transmembrane; VMD, visual molecular dynamics; RMSD, root-mean-square deviation; RMSF, root-mean-square fluctuation; G_t, G-protein transducin.

10.1021/bi0506019 CCC: $30.25
Published on Web 08/30/2005

Subsequently, photorhodopsin thermally relaxes within a few picoseconds to a distorted all-*trans* configuration, bathorhodopsin (*17*). In bathorhodopsin, the chromophore is expected to retain the energy of the photon, because it does not have the time to relax. Models for energy storage in bathorhodopsin suggest that absorbed energy can be stored through (i) structural changes in the retinal chromophore itself, (ii) alterations in the interactions between the retinal and its protein environment, or (iii) a combination of both. Calorimetric, nuclear magnetic resonance (NMR), infrared, and Raman studies of bathorhodopsin at low temperature suggest that the distortion in the conformation of the chromophore accounts for an important part in photon-energy storage (*17*−*24*). An early NMR study on bathorhodopsin suggested that the energy stored in the primary photoproduct does not induce any substantial changes in the average electron density of the polyene chain, which is similar to the dark-adapted state and to isorhodopsin (*24*). Vibrational spectroscopy studies at low and at room temperature confirm that the vibrational modes in the Schiff-base region of the retinal chromophore in the dark-adapted state of rhodopsin are unchanged upon bathorhodopsin formation (*23*, *25*). The charge separation between the Schiff base and its counterion, therefore, does not make a major contribution to this part of the energy storage/transduction mechanism. Furthermore, significant changes between the dark-adapted state and bathorhodopsin occur in the polyene chain, indicating substantial twisting of the retinal backbone at low temperature ($T <$ 100 K) and at room temperature (*17*, *21*, *23*, *25*, *26*).

On a nanosecond time scale [∼120 ns (*27*)], bathorhodopsin establishes an equilibrium with a blue-shifted intermediate (BSI) before the mixture decays to form lumirhodopsin (in ∼150 ns (*27*)]. BSI is not observed under cryogenic conditions but rather observed by flash photolysis at ambient temperature (*28*). The equilibrium between bathorhodopsin and BSI is independent of the protein environment but can be influenced by chemical modification of the retinal, suggesting that the bathorhodopsin to BSI only involves conformational changes of the chromophore (*10*). The proposed barrier for the formation of BSI is the steric interaction between H8 (hydrogen atom on carbon C8 of the retinal) and the C5 methyl group of retinal (*29*, *30*).

The decay from BSI to reach lumirhodopsin in the nanosecond time scale can be significantly affected by the amino composition of the binding pocket but not by the chromophore (*10*, *31*). Therefore, it seems that this step involves the adjustment of the protein matrix to the isomerized chromophore (*10*). In the lumirhodopsin state, the salt bridge between the protonated Schiff base and Glu113 is broken and retinal is believed to be fully relaxed (*11*). Breaking the salt bridge decreases the pK_a of the protonated Schiff base, facilitating the transfer of the proton to Glu113 at a later stage (*32*, *33*).

Lumirhodopsin is then transformed into metarhodopsin I and subsequently to metarhodopsin II, where important conformational changes take place in the protein and the active conformation for G-protein coupling is reached (*10*). The ^{13}C NMR chemical shifts of the retinal provide convincing evidence that Schiff-base deprotonation occurs in the transition between metarhodopsin I and II (*34*), as suggested by the pH dependence of the UV/vis spectrum observed for the metarhodopsin I state (*35*).

Rhodopsin is the only GPCR for which accurate structural information is available. Several crystal structures are available (*36*, *37*), even indicating the position of hydration water within the protein in the most recent ones (*38*−*40*). These structures have been complemented recently by a structure of the active state, metarhodoposin II (*41*). The availability of this structural information has enabled various theoretical studies, including MD (*42*−*45*) and quantum simulations on fragments of the protein [using the Density Function Theory (DFT), for example] (*39*, *46*−*49*).

Whereas the crystallographic data reveals a detailed description of the receptor in the inactive dark state and, until recently, low-resolution information on the chromophore, solid-state NMR provides accurate structural and electronic information on the chromophore, both in the dark-adapted state and in one of its photointermediate states. Rotational resonance has been used successfully to provide selected internuclear distances or restraints in the dark-adapted state, metarhodopsin I and II (*50*−*53*). The validity of the method was confirmed for the dark-adapted state with data from an improved X-ray crystal structure (*39*). Furthermore, the analysis of the chemical shift at various photoactivated states and their comparison with Schiff-base models or rhodopsin-bound retinal in the dark state can be used to probe the electronic environment around the isotopic labels selectively inserted in the chromophore (*24*, *34*, *54*−*58*).

Previous MD simulations of bovine rhodopsin have focused mainly on conformational fluctuations at the level of the protein, either in the dark-adapted state (*44*, *45*) or after isomerization of the chromophore (*42*, *43*). In one using the amber force field, a change in protein structure was observed 1.75 ns after the isomerization of the retinal was induced; the protein was in an octanol layer surrounded by water as a membrane mimetic (*42*). In another, using NAMD, changes in retinal were monitored over 1 ns and more gradual changes in protein structure were observed over 10 ns. In this study, the protein was embedded in a palmitoyl-oleoyl-phosphatidylcholine bilayer of 108 lipids and surrounded by water for the MD (*43*). These studies are based on the 1HZX crystal structure (*59*) and released before accurate data for the chromophore were made available. In a recent study, Röhrig et al. (*60*) focused on the first 0.5 ps, using a hybrid quantum mechanical/molecular mechanical MD calculation. Events in the first 0.5 ps were observed in the polyene chain. Again, 1HZX was used. Here, we present a computational study of bovine rhodopsin inserted in an explicit membrane environment (Figure 1), focusing on the structural and dynamic properties of the chromophore in the protein. Both the dark-adapted state and the early stages after retinal isomerization have been studied. Specifically, this contribution endeavors to refine the mechanism for signal propagation within the chromophore after absorption of a photon and transmission to the protein structure of that light signal based on recent structural information of the protein.

The theoretical study here provides a model reflecting the dynamics and conformation of retinal bound to bovine rhodopsin in the dark-adapted state and in states after light activation but before BSI (which MD simulation cannot reach because of the excessive computational time required). Furthermore, the use of different initial conditions for the isomerization illustrates the stochastic nature of the activation process at the level of the retinal. It has therefore been pos-

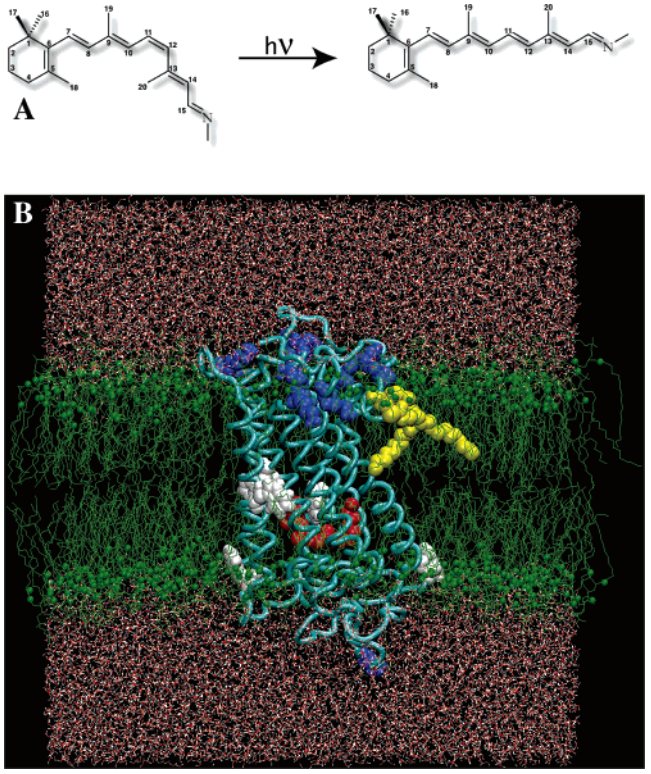

FIGURE 1: (A) Chemical structure of 11-*cis*-retinal and all-*trans*-retinal. (B) Illustration of the simulation box (blue, lysine; green, POPC; red, lysine-bound retinal; white, tryptophan; yellow, palmitoylated cysteine; red and white, water).

sible to carry out MD simulations on a physiologically comparable time scale for the isomerization of the retinal chromophore and compare the simulation with experimental data.

MATERIAL AND METHODS

MD Calculations. MD simulations were performed with the GROMACS version 3.1.5 package, using gromos43A2, extended to improve the simulation of the lipid components for the force field (*61*). Simulations were run at a temperature of 300 K and a pressure of 1 bar in an isothermal−isobaric ensemble (NPT) with periodic boundaries present. Both Berendsen temperature and pressure couplers were chosen to keep these parameters constant. The time step for the simulations was 1 fs in the case of the short 5-ps MD simulations and 2 fs for the others. A LINCS algorithm was used to maintain the geometry of the molecules. Long-range electrostatic interactions are calculated with the particle-mesh Ewald (PME) method. PME tends to slow the computation but increase its quality because it removes any cutoff electrostatic interactions. Lennard−Jones interactions were cut off at 1.4 nm. The single-point charge (SPC) water model (*62*) was used to describe the water in the simulation box.

Lipids. The bilayer consisted of a 1-palmitoyl-2-oleoyl-*sn*-glycerophosphocholine (POPC) patch including initially 288 lipids and 16 337 water molecules. The topology file for the POPC molecule had been previously described and was available from http://moose.bio.ucalgary.ca/Downloads.

Protein. A crystal structure of the dark-adapted state rhodopsin (chain A, 1L9H from PDB) was used as a starting point for building the molecular model of the protein. Missing residues in the intracellular loops were added using Modeller (*63*). The simulation of rhodopsin involves two functionalized amino acid residues, palmitoylated cysteine and retinal-bound lysine, for which it was necessary to write a molecular description. The parameters used to simulate the palmitoyl chains were based on the parameters used to simulate the lipids.

Retinal. Retinal was carefully parametrized to reproduce experimental data previously gathered for retinal in the dark-adapted state (*51*, *64*−*66*) in the gromos43a2 force field (see Tables 1S and 2S in the Supporting Information). The parametrization was based on a previous DFT theoretical study on 6-*s*-*cis*-retinal (*48*) and is in agreement with a recent 0.22 nm resolution crystal structure (*39*). The bond lengths, bond angles, and dihedral angles from this model have been used as parameters for the retinal topology (Table 1S in the Supporting Information). The partial charges on the nuclei were approximated on the basis of the Mulliken charges of the DFT model (Table 2S in the Supporting Information). The 6-*s*-*cis* conformer and dihedral angle equilibrium values (Table 1S in the Supporting Information) proposed by Sugihara et al. (*48*) were used as the starting conformation for retinal in rhodopsin and used to replace the chromophore present in the 1L9H crystal structure. This approach encompasses the experimental and other observations of extensive electron delocalization over the retinal polyene chain [Smith et al. (1985) *Biophys. J. 47*, 653−664; Lee, et al. (2002) *J. Chem. Phys. 116*, 6549].

Insertion of the Protein into the Bilayer and Equilibration. The protein was inserted in the bilayers using a method that generates a suitable cavity in the interior of the lipid bilayer (*67*) based on the solvent-accessible surface of the protein used as a template during the course of a short steered MD simulation (SMD) of a solvated lipid membrane (500-ps SMD run). The protein−lipid equilibration was achieved through a three-stage process. First, overlapping water molecules were removed, and then lipid molecules whose headgroups are located within 0.15 nm from the protein surface were removed; the protein−lipid interface was optimized by applying repulsive forces perpendicular to the protein surface, to the remaining lipid atoms inside the volume occupied by the protein until it was emptied. The protein itself was then inserted into the bilayer. Counterions were added to maintain the electroneutrality of the simulation box. The system was energy-minimized at each step that involved the addition or removal of any molecular species (steepest descent algorithm). Finally, the system was equilibrated in successive short MD simulations (5 runs of 200 ps each), where position restraints were applied to the protein and progressively decreased. The minimum distance between the protein and its mirror images is at least 2.5 nm at anytime of the simulations.

MD Runs. One 10-ns MD simulation was run for the dark-adapted state, while the isomerization of the chromophore was studied in a series of six MD simulations (Figure 2): three 5-ps simulations with a 1-fs time step, where frames were collected for every time step of the calculation, directed toward the first picoseconds of the isomerization, and three 10-ns simulations with a 2-fs time step, intended to follow the interactions between retinal and its binding pocket. Photoactivation of retinal was simulated using SMD techniques previously described (*42*, *43*), where the dihedral parameters for the 11-*cis* bond were switched to describe a *trans* double bond.

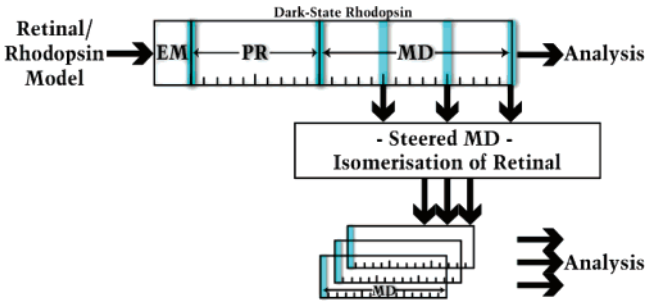

FIGURE 2: Strategy to study the isomerization of retinal. A 10-ns MD of bovine rhodopsin is run to generate frames used as the starting conformation for the isomerization (including starting velocities). Frames after 500, 1000, and 1500 ps were used as seeds for SMD simulations, where retinal is isomerized from 11-*cis* to all-*trans*. The interpretation is based on the comparison between the SMDs, where retinal is isomerized with the MD of bovine rhodopsin in its dark-adapted state.

Computers. MD simulations were run on various computers including a PowerBook G4 running under Mac OS X (1.25 GHz, 512 MB RAM) for the shortest MDs and the data analysis or an 8 processor Beowulf-class cluster made of 4 dual processor X-serve G4 rack units (2 × 1.25 GHz, 1 GB RAM) with GHz switches and UPS, running under a Mac OS X (10.2.8). MD calculations were run using simultaneously several processors (2 or 4) with the MPI middleware distributing the processes over all units.

Data Analysis. For the analysis (tilt, kink angle, etc.), only the core residues of the transmembrane (TM) helices were included: (H1) 35−64, (H2) 72−98, (H3) 109−138, (H4) 151−172, (H5) 201−225, (H6) 245−277, and (H7) 286−308. The retinal binding pocket was defined as the amino acids present within 0.45 nm from the retinal as described by Palczewski et al. (*36*). All molecular structures were drawn using visual molecular dynamics (VMD) (*68*).

RESULTS AND DISCUSSION

Data obtained by vibrational spectroscopy provides information on the chromophore, which is difficult to translate into an accurate molecular description of interatomic distances, while structural approaches such as X-ray and NMR provide a few accurate snapshots on the molecular conformation of the chromophore in various states of the protein-activation pattern. MD simulation is a tool with the potential of linking these two important experimental contributions, at least on a short time scale (∼10 ns) and can then be tested.

The 10-ns MD simulation of bovine rhodopsin in the dark-adapted state shows a distorted retinal in a relatively rigid binding pocket. The isomerization takes place in a 100-fs scale (*15*) and is followed by several conformational changes within retinal at the pico- and nanosecond time scale. At a 10-ns time scale, most of the changes deriving from the isomerization take place in the retinal itself. A comparison of the motion of the protein in general and the motion of the residues involved in the binding pocket on a 10-ns time scale does not show large-amplitude conformational changes that can be directly linked with the isomerization of retinal and interpreted as the protein response to the retinal isomerization.

Rhodopsin in the Dark-Adapted State. During the 10-ns MD in the dark-adapted state, the root-mean-square deviation

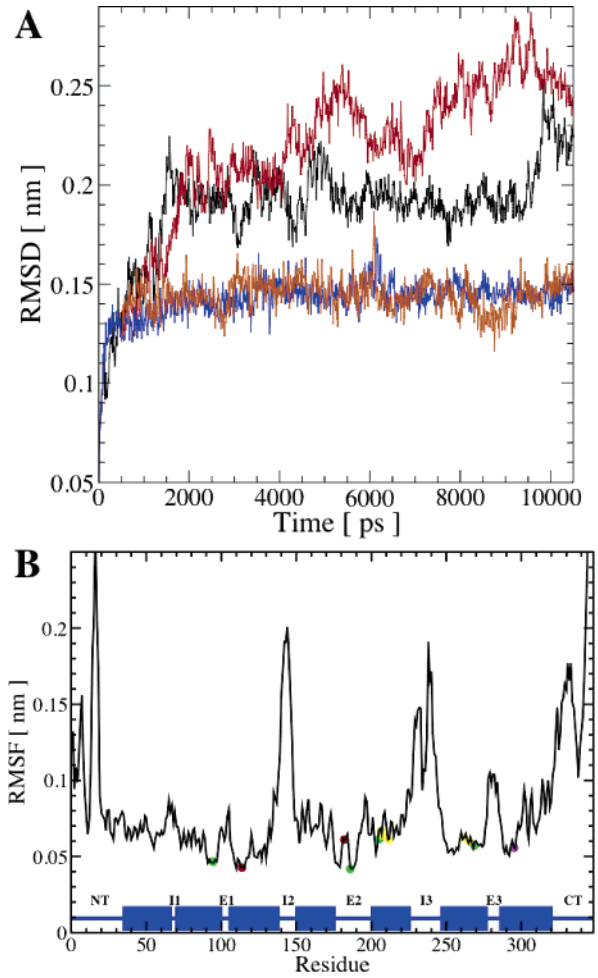

FIGURE 3: (A) Backbone RMSD of bovine rhodopsin in the dark-adapted state (black) and after isomerization of the retinal (red, starting point = dark-adapted state trajectory, after 500 ps). RMSD curves of the residues belonging to the binding pocket are also displayed for the dark-adapted state (blue) and after isomerization (orange). (B) RMSF of rhodopsin in the dark-adapted state. The secondary structure is highlighted in blue at the bottom to show the position of the TM helices; residues in retinal binding pocket are marked (red = negative, yellow = aromatic, and green = positive).

(RMSD) of rhodopsin increases quickly to reach an average value of about 0.2 nm, around which it oscillates during the remainder of the simulation (Figure 3). The RMSD computed for the residues from the binding pocket show a different value, close to 0.15 nm. The comparison between the two RMSD curves indicates that most of the motion in the protein takes place in the loops. This was confirmed by the root-mean-square fluctuations (RMSF values) computed for the protein residues (Figure 3), where the highest values are obtained for the intracellular loop and the C-terminal domain. Analogous behavior has been observed experimentally by X-ray crystallography, where high-temperature (B) factors were reported for the loops and as a result some loop structures are missing in the earliest crystal structures (*36*, *40*, *59*).

Modeling 11-cis-Retinal in the Dark-Adapted State. The retinal model was parametrized on the basis of a theoretical contribution where the conformation of 11-*cis*-retinal in the binding pocket was determined using DFT for the value at equilibrium of all parameters and using standard values from the force field (*48*). The dihedral interactions for all of the

Table 1: Distance Restraints within Retinal for Rhodopsin in the Dark-Adapted State Determined by MD at 300 K, DFT, and $^{13}C-^{13}C$ Rotational Resonance NMR at 210 K

atom pair	C10−C20	C11−C20	C8−C16	C8−C17	C8−C18
MD distance[a] (nm)	0.309 ± 0.014[b]	0.306 ± 0.001[b]	0.442 ± 0.010[b]	0.388 ± 0.017[b]	0.308 ± 0.013[b]
DFT distance (nm)	0.307	0.309	0.435	0.398	0.300
reference	*48*	*48*	*48*	*48*	*48*
NMR distance (nm)	0.304 ± 0.015[c]	0.293 ± 0.015[c]	0.405 ± 0.025[c]	0.405 ± 0.025[c]	0.295 ± 0.25[c]
reference	*64*	*64*	*51*	*51*	*51*
X-ray distance (nm)	0.329 ± 0.00[d]	0.325 ± 0.00[d]	0.448 ± 0.036[d]	0.446 ± 0.034[d]	0.328 ± 0.008[d]
reference	*39*	*39*	*39*	*39*	*39*

[a] Averages of a set of three MDs of the same duration. [b] Standard deviation of the fluctuations during the MD. [c] Experimental error. [d] ±Standard deviation on chains A and B.

Table 2: Distance Restraints within Retinal for Rhodopsin Determined by MD within 10 ns after the Isomerization of Retinal at 300 K and $^{13}C-^{13}C$ Rotational Resonance NMR for Metarhodopsin I at 210 K

atom pair	C10−C20	C11−C20	C8−C16	C8−C17	C8−C18
MD distance[a] (nm)	0.444 ± 0.014[b]	0.305 ± 0.009[b]	0.439 ± 0.011[b]	0.396 ± 0.017[b]	0.332 ± 0.017[b]
	0.444 ± 0.011[b]	0.304 ± 0.009[b]	0.439 ± 0.010[b]	0.398 ± 0.017[b]	0.315 ± 0.015[b]
	0.448 ± 0.011[b]	0.308 ± 0.009[b]	0.442 ± 0.012[b]	0.390 ± 0.016[b]	0.341 ± 0.013[b]
	(0.445 ± 0.013)	(0.306 ± 0.009)	(0.440 ± 0.011)	(0.395 ± 0.017)	(0.329 ± 0.015)
NMR distance (nm)	0.435 ± 0.015[c]	0.283 ± 0.015[c]	NA	0.405 ± 0.025[c]	0.295 ± 0.025[c]
reference	*64*	*64*		*52*	*52*

[a] Averages of a set of three MDs of the same duration. [b] Standard deviation of the fluctuations during the 10-ns MD. [c] Experimental error.

bonds in the polyene chain were set with the standard values used for double bonds to give the model the rigidity required to reproduce accurately information derived from the experiment [i.e., interatomic distances measured by solid-state NMR (*51*)]. This parametrization gave a model for the chromophore that reproduces reasonably well the structural information available (*39*, *51*, *52*).

Rotational resonance solid-state NMR was used for distance determinations within the rhodopsin-bound chromophore in membranes for the dark-adapted state and metarhodopsin I (*51*, *64*) (Tables 1 and 2). From these distances, it was shown that the C10−C13 unit is conformationally twisted (*64*). Rotational resonance solid-state NMR was also used to provide distance restraints regarding the relative orientation between the β-ionone ring and the polyene chain of the chromophore in rhodopsin (*51*). The distances measured between C8−C16, C8−C17, and C8−C18 show that the major portion of retinylidene in rhodopsin has a twisted 6-*s*-*cis* conformation (*51*).

One of the goals of this study was to implement an accurate retinal model to be used for MD simulations of bovine rhodopsin in the dark-adapted state. For this purpose, the distance restraints defined by solid-state NMR constitute an important block of experimentally derived structural information. Table 1 include the averages for the corresponding distances as computed from our theoretical model, while Figure 4A displays the instantaneous distance as a function of the simulation time. The comparison shows good agreement between the model and the experimental data from both NMR and X-ray (Table 1). A further comparison with NMR data shows only one distance that is 0.012 nm at variance with the simulation from the error range of the NMR determination. Table 3 and Figure 5 show an analogous comparison of the MD-derived model for selected dihedral angles, showing a close agreement between the model and NMR-derived distances (note that the temperature between the experiment and simulation differs by 70 K). The averaged distances are also fluctuating and are close to the values defined by the DFT-derived 6-*s*-*cis* conformer (*48*).

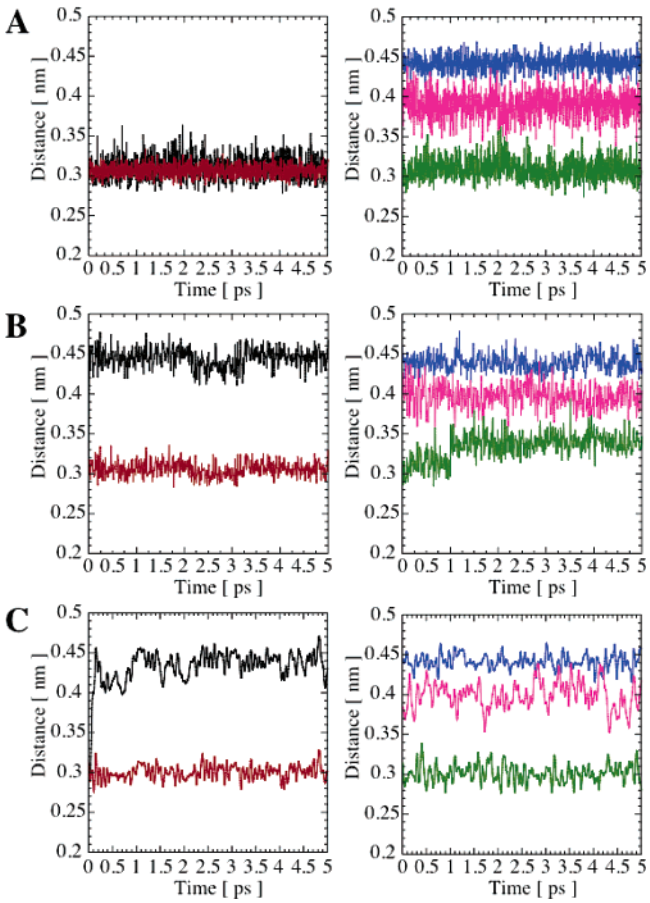

FIGURE 4: Illustration of intramolecular distances within retinal, experimentally measured by solid-state NMR in the dark-adapted state and in metarhodopsin I: C10−C20 (black), C11−C20 (red), C8−C16 (blue), C8−C17 (fuchsia), and C8−C18 (green). (A) 10-ns MD in the dark-adapted state. (B) Example of a 10-ns MD, where the isomerization of retinal is initiated at time = 0 ps (500-ps MD in the dark-adapted state was run previously). (C) Same as B with a simulation time of 5 ps.

While setting-up a model for retinal permits a more accurate description of a crucial fragment of rhodopsin for

Table 3: Dihedral Angles for Selected Bonds for Retinal in the Dark-Adapted State, Determined by MD, DFT, and NMR at 210 K

dihedral angle	MD average[a]	DFT	NMR	X-ray
C5−C6−C7−C8	−39 ± 9°[b]	−35°	−28 ± 7°[c,d] (*51*)	38 ± 3°[e]
C10−C11−C12−C13	−20 ± 11°[b]	−12°	±44 ± 10°[c,d] (*64*)	−31 ± 1°[e]
C8−C9−C10−C11	166 ± 11°[b]	175°	160 ± 10°[c] (*76*)	−176 ± 0.3°[e]
C13−C14−C15−NZ	180 ± 15°[b]	173°	165 ± 5°[c] (*77*)	172 ± 10°[e]

[a] Averages of a set of three MDs of the same duration. [b] Standard deviation of the fluctuations during the MD. [c] Experimental error. [d] NMR-based estimations are based on the 11-*cis*-retinal crystal structure for which the bond angle was rotated to match $^{13}C-^{13}C$ rotational resonance distances. [e] Average ± standard deviation on chains A and B.

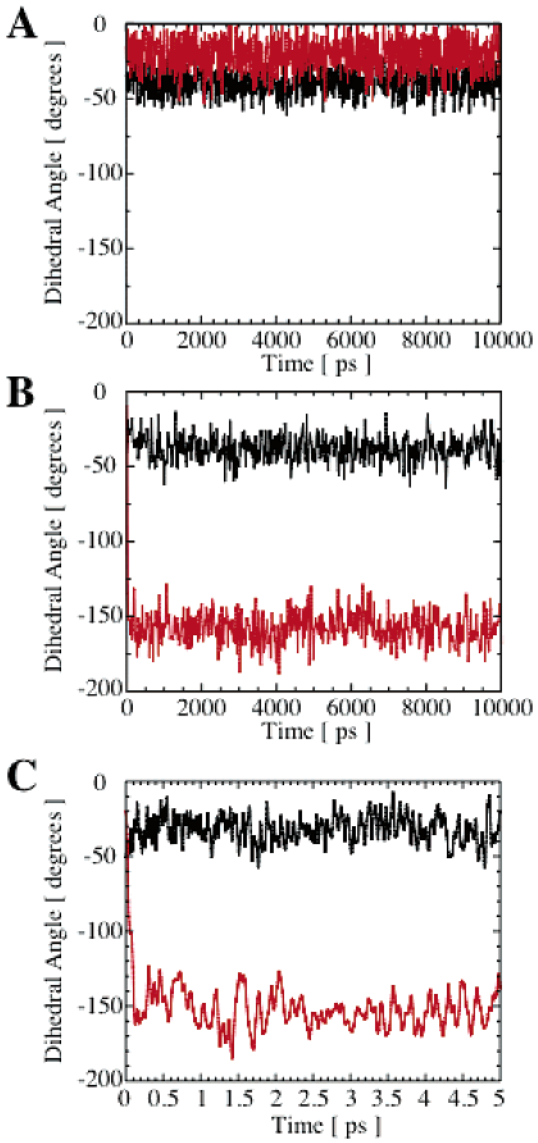

FIGURE 5: Dihedral angle C5−C6−C7−C8 (black) and C10−C11−C12−C13 (red) for (A) retinal bound to rhodopsin in the dark-adapted state, (B) 10-ns MD describing the isomerization of retinal after 500-ps MD in the dark-adapted state, and (C) 5-ps MD describing the isomerization of retinal after 500-ps MD in the dark-adapted state.

MD, it also allows a more accurate investigation of the dynamics of the chromophore in its binding-pocket and can be applied for the further investigation of rhodopsin mutants in the dark-adapted state.

Various parameters are useful for characterizing the dynamics of the retinal model in the dark-adapted state. The RMSF is one of them (Figure 6), highlighting among other things that the methyl groups are the most mobile parts of the chromophore and that both C11 and C12 are the atoms

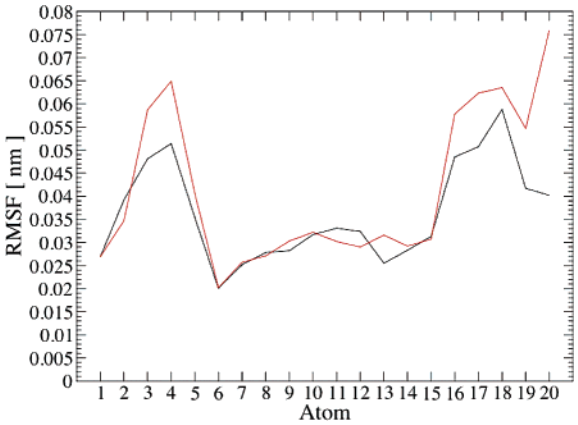

FIGURE 6: RMSF for retinal, illustrating the increased vibrations at the level of selected parts of retinal after isomerization (black, dark-adapted state; red, after isomerization). Atoms 3−5 from the β-ionone ring (in contact with helix V) and all methyl groups (atoms 16−20) show a visible increase of their corresponding RMSF upon isomerization.

within the polyene chain that fluctuate the most around their average location. The standard deviations of various averaged interatomic distances and dihedral angles are also good indicators of the retinal dynamics. For the model in the dark-adapted state, the standard deviations for the distance between nondirectly bonded atoms, e.g., C8−C18 (Table 1), were below 0.02 nm. At the same time, dihedral angles exhibit a standard deviation around 10°, which can significantly affect the local geometry of the molecules. This model sets the picture of retinal as a rather twisted and flexible molecule, while maintaining some interatomic distances relatively fixed (fluctuations are less than 5% of the average value, Table 1).

The RMSD computed for the lysine-bound retinal (Figure 7A, black) fluctuates around 0.08 nm, which is even lower than the average RMSD for the binding pocket (Figure 3A). rmsd computed for various fragments shows that most of the deviation from the structure of the reference [retinal conformer derived by DFT (*48*)] occurs in the polyene chain (Figure 7A, blue), while the deformation of the ring geometry is less affected, with the exception of the methyl groups present on the ring (RMSF, Figure 6, black).

Transition from 11-cis to All-trans-retinal. The isomerization of retinal has been studied in two groups of short 5-ps MDs and long 10-ns MDs, each containing three simulations starting from a different starting point. The starting point for each of the MDs was taken from the 10-ns MD of rhodopsin in the dark-adapted state respectively at time 500, 1000, and 1500 ps (Figure 2).

The choice of two time-scales results from a technical compromise: to follow accurately the isomerization of retinal at the femto- to picosecond level, the output of a large

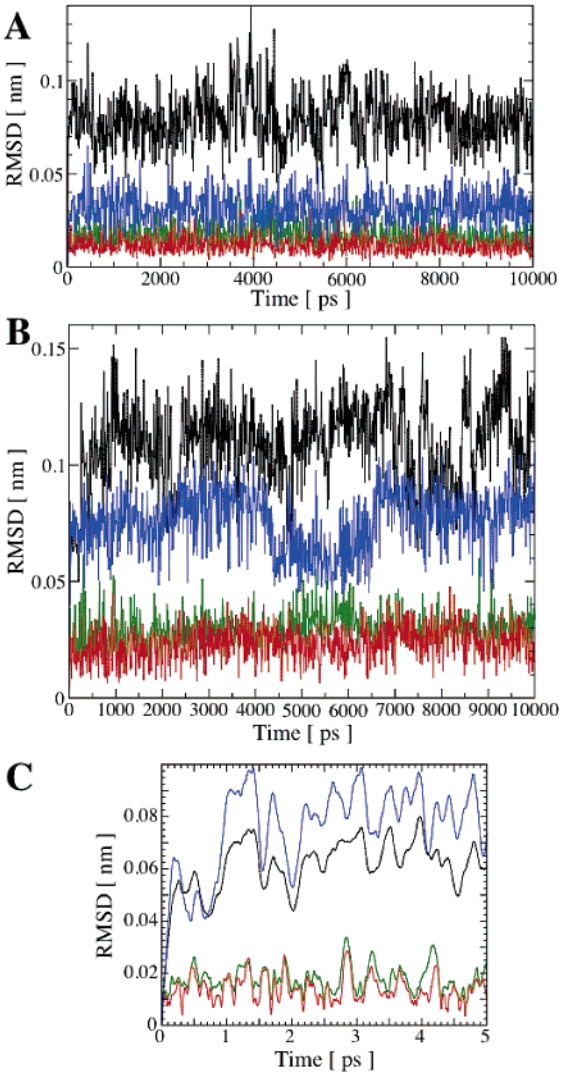

FIGURE 7: RMSD for the lysine-bound retinal (black) and fragments of the retinal−β-ionone ring (red), β-ionone ring and C7−C8 (green), and polyene tail (blue). (A) Dark-adapted state. (B) 10 ns after isomerization of retinal after 500-ps MD in the dark-adapted state. (C) First 5 ps after isomerization of retinal, after 500-ps MD in the dark-adapted state.

number of frames with a very short time step is required (time step = 1 fs, frame saved every calculation step). This approach is not practicable for larger simulations, with the space for storing the data and the RAM memory required for the analysis being prohibitive. As a result, these long-term MDs use a slightly different setup (time step = 2 fs, frame saved every 500 calculation steps) to explore longer simulation times at the expense of time resolution.

The isomerization was induced by switching the potential function describing the dihedral interaction for the 11-*cis* bond. This approach has been described in detail in previous reports (*43*, *69*). The force field used can be expected to include fully the essential steric and electrostatic effects. However, it has some limitations. One of them is the use of united pseudoatoms for aliphatic apolar hydrogen atoms, which are not explicitly described. A consequence of this approach is to attenuate the distribution of partial charges on the atoms. As previous studies have shown that the changes in the partial charges upon isomerization are rather small, with a maximum of 0.1 e between the 11-*cis* to the all-*trans* (*43*), the same partial charges were used to describe retinal in the dark-adapted and photoactivated states.

Table 4: Dihedral Angles for Selected Bonds for Retinal after the Isomerization, Determined by 10-ns MD within 2 ns after the Isomerization of Retinal at 300 K, and NMR for Retinal in Metarhodopsin I at 210 K

dihedral angle	MD average[a]	NMR
C5−C6−C7−C8	−38 ± 9°[b]	−28 ± 7°[c,d]
	−36 ± 9°[b]	
	−38 ± 9°[b]	
	(37 ± 9°)	
C10−C11−C12−C13	−157 ± 12°[b]	NA
	−162 ± 12°[b]	
	−159 ± 12°[b]	
	(159 ± 12°)[b]	
C9−C10−C11−C12	176 ± 13°[b]	180 ± 15°[c]
	171 ± 16°[b]	
	175 ± 11°[b]	
	(174 ± 14°)	

[a] Averages of a set of three MDs of the same duration. [b] Standard deviation of the fluctuations during the MD. [c] Experimental error. [d] NMR-based estimations are based on the 11-*cis*-retinal crystal structure for which the bond angle was rotated to match $^{13}C-^{13}C$ rotational resonance distances.

A comparison of the rmsd curves for rhodopsin (Figure 3A) shows that the isomerization of retinal leads the protein on a different path during the MD from the one followed in the dark-adapted state (note that the reference for all rmsd curves is the same: the conformation of the protein at time = 0 of the MD simulation in the dark-adapted state). From the RMSF plot, most of the motions taking place in the protein are located near the loops (data not shown), in particular, the intracellular loops and the C-terminal domain of the protein, in a scheme similar to the dark-adapted state simulation.

The results presented here illustrate the path followed by the molecular model of retinal upon isomerization. The results strongly suggest that the followed path depends on both starting coordinates and velocities of the retinal. Only a few of the many available paths have been followed for a relatively short time; therefore, this analysis cannot be exhaustive but should rather be interpreted semiquantitatively.

Dynamics of the Isomerization and Pattern of Activation. The isomerization of the model was followed by monitoring the dihedral angle of the C10−C11−C12−C13 bond as a function of time (Figure 5C for a detailed description of the first 5 ps and Table 4). From the three 5-ps MDs, the isomerization of the chromophore starts within 50 fs after the isomerization is initiated and takes about 150−200 fs depending on the starting conformation for the retinal to isomerize around the C11−C12 bond in close agreement with spectroscopic experiments (*15*). In addition, the different conformations generated by each of the MD simulations were clustered using a full linkage algorithm (and a cutoff of 0.007 nm, Figure 8). This type of analysis simplifies the visualization of the conformation changes within retinal and identifies in all three simulations a short-lived cluster with a lifetime of about 50−800 fs (range derived from the three MDs), where the C11−C12 bond has been isomerized without the rest of the polyene chain having the time to rearrange. From the time scale and the nature of the conformational change, it is tempting to associate these clusters with the photor-

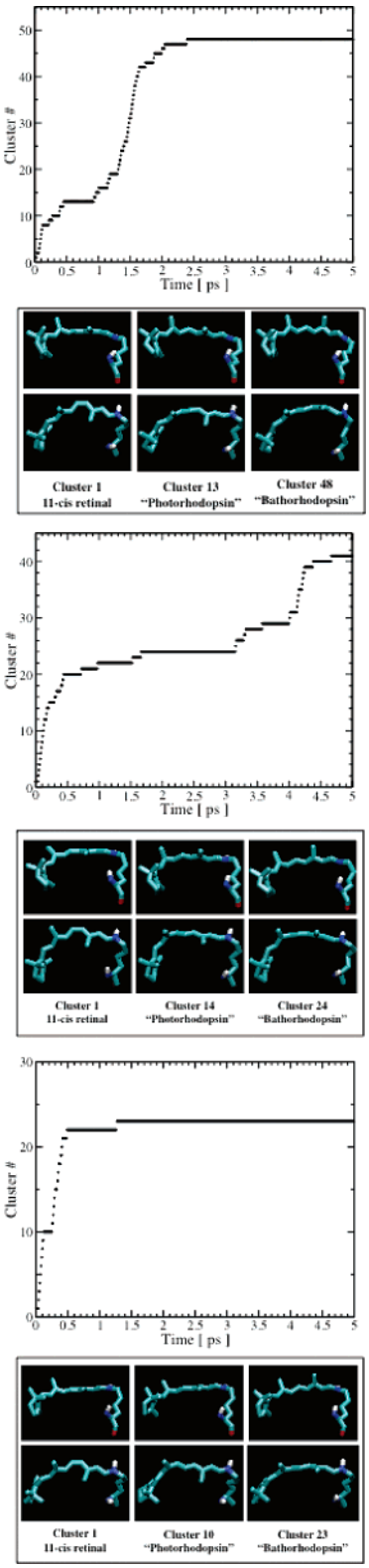

FIGURE 8: Cluster analysis on several 5-ps MD simulations each from different starting points. Retinal is isomerized in bovine rhodopsin initially in the dark-adapted state. Starting conformations come from different snapshots of the dark-adapted state. A clustering algorithm is used to follow conformational changes in the molecule. Conformations are sampled every 1 fs from the trajectory, and a full-linkage algorithm with a 0.007 nm cutoff is used.

hodopsin intermediate. Further, the very short lifetime of these clusters offers an explanation of why it is not possible to isolate this photointermediate (*15*).

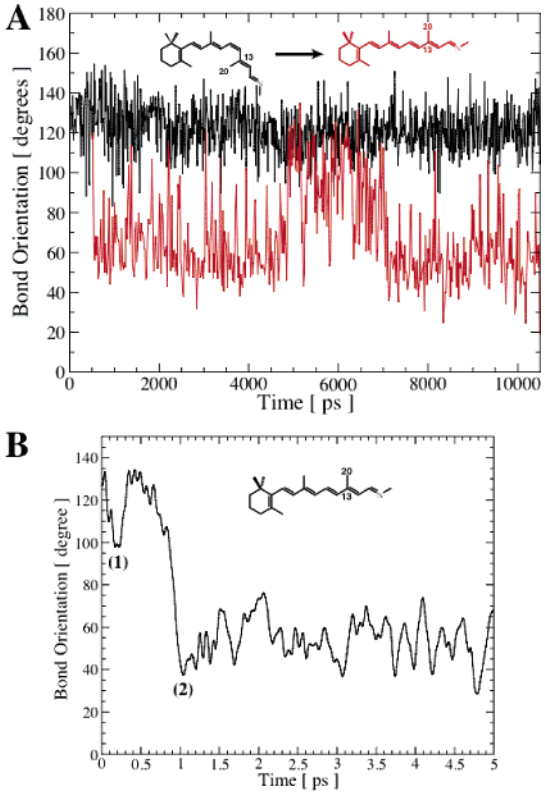

FIGURE 9: Angle of bond C13−C20 with the *z* axis (normal to the membrane plane), showing a large-scale rotation of methyl group C20 upon isomerization (70−90°, depending on the starting conformation). (A) 10-ns MD of bovine rhodopsin in the dark-adapted state (black) and after isomerization of retinal (red), after 500-ps MD in the dark. (B) 5-ps MD of bovine rhodopsin after isomerization of retinal (isomerization initiated after 500 ps in the dark). (1) Point corresponding to the end of the isomerization of the C11−C12 double bond, interpreted as being "photorhodopsin". (2) Point corresponding to the flip of methyl-C20, interpreted as being "bathorhodopsin". The bond orientation is given related to the normal to the membrane plane, with 0° corresponding to a vector pointing toward the extracellular side and 180° corresponding to a vector pointing toward the cytoplasmic side of the membrane.

Another important conformational change that occurs within the first few picoseconds after the isomerization is initiated is the rotation of the methyl group C20. The rotation of the methyl group takes place along an axis, which is approximately normal to the membrane plane. The angle defined by the bond vector C13−C20 and the *z* axis of the simulation box is adequate to follow the orientation of the bond inside the binding pocket. Figure 9B presents an example of the rotation that the methyl group undergoes, where it takes about 1 ps for the rotation to be completed. The average time needed for the rotation to take place over the three 5-ps MD is 1.33 ps (1.5/1/1.5 ps) and the average amplitude of the rotation is 95° (100°/93°/93°). Further cluster analysis identifies clusters (Figure 8) that appear shortly after the methyl group has flipped over, strongly suggesting this state is related to bathorhodopsin.

Altogether, the time scale and the amplitude of the various conformational changes observed within the chromophore during the first 5 ps after isomerization suggests that they may be related with the previously identified photointermediates photorhodopsin and bathorhodopsin. In addition, the isomerizations from several slightly different conformations for the 11-*cis*-retinal leads to a distribution of the time

Table 5: Intramolecular Distances Illustrating the Length Extension of Retinal upon Isomerization[a]

intramolecular distances	dark-adapted state	after isomerization[b]	crystallized all-*trans*-retinal
C13−C4 (nm)	0.881 ± 0.031[c]	1.016 ± 0.033[d]	1.148
		1.016 ± 0.034[d]	
		0.992 ± 0.042[d]	
		(1.008 ± 0.036)	
C15−C4 (nm)	1.044 ± 0.041[c]	1.187 ± 0.048[d]	1.355
		1.192 ± 0.044[d]	
		1.150 ± 0.055[d]	
		(1.176 ± 0.051)	

[a] The corresponding distances are longer in the crystallized all-*trans*-retinal, suggesting that the chromophore can extend more. [b] Averages of a set of three MDs of the same duration. [c] Average on a single 10-ns MD of bovine rhodopsin in the dark-adapted state. [d] Average on the three 10-ns MD of bovine rhodopsin after isomerizaiton of retinal.

required for transition from one photointermediate to another (i.e., and the conformational changes that they imply). This is interpreted as the existence of multiple pathways leading to the activation of the protein and might explain the coexistence of several photointermediate states. Nevertheless, the sequence of the observed conformational changes remains the same in all of the simulations.

To extend the three short 5-ps MD described in the previous paragraphs, three longer 10-ns MD simulations have been run, starting from the same points of the trajectory where rhodopsin was simulated during 10 ns in the dark-adapted state, These MDs explore the conformational changes taking place in retinal on a much longer time scale. These changes are not localized, as are the earliest changes within the chromophore, but rather involve the entire retinal molecule and are more subtle. A careful comparison with the 10-ns MD of rhodopsin in the dark-adapted state was required to ensure that it results from the isomerization and not from thermal fluctuations.

Among these changes is an extension of the retinal length by about 0.1−0.14 nm, which can be tracked by following the interatomic distance between either C13 or C15 and C4 (Table 5). Another conformational change is the increase of the interatomic distance between C8 and C18, by a modest 0.02 nm, as a result from a slight change in the orientation of the ring (Figure 4B). The methyl groups undergo increased fluctuation (Figure 6), which can affect their average orientation (Figure 9).

Further cluster analysis performed simultaneously on all 10-ns MD (Figure 10) shows that retinal in both the dark-adapted state and after isomerization is segregated in two distinct clusters. For both states, 78% of the conformation can be gathered in one cluster with a cutoff of 0.0021 nm (no cluster visible with a cutoff lower than 0.0018 nm). This means that, within 10 ns, retinal does not fluctuate more than ∼0.02-nm rmsd away from its average conformation. Furthermore, the amplitude of the fluctuations seems to be the same for retinal in the dark and retinal after isomerization; i.e., on the nanosecond time scale, conformational changes are driven mainly through thermal fluctuations or perturbations that have a similar amplitude.

Relaxation of the Binding Pocket. A general feature of the retinal model after isomerization is an increase in the vibrational fluctuations of some fragments of the molecule. These fluctuations are highlighted in Figure 7B, with an

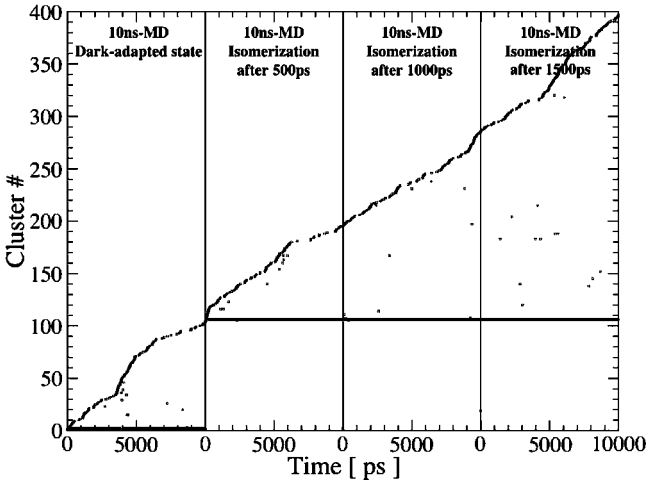

FIGURE 10: Cluster analysis on several of the 10-ns MD simulations. Conformations are sampled every 20 ps from the trajectory (a total of 2000 conformations analyzed), and a full-linkage algorithm with a 0.021 nm cutoff is used. Two main clusters can be identified, with cluster 2 gathering 78% of the retinal conformers in the dark-adapted state and cluster 106 also gathering 78% of the retinal conformers after isomerization.

increased fluctuation in the rmsd plot compared to the dark-adapted state (Figure 7A). Furthermore, the RMSD plot for retinal after isomerization (Figure 6) highlights the methyl groups (C16−C20) and atoms C3−C4 from the β-ionone ring, as the positions in the chromophore where increased vibrational activity takes place. This vibration results from the process of reciprocal adaptation between the chromophore and its binding pocket after the isomerization. A transfer of this vibrational activity could take place between the retinal and its binding pocket. Figure 11B illustrates this at the level of the β-ionone ring, where the time fluctuations for distance between the ring and the surrounding residues increase and can possibly act as a way to transfer the signal from the retinal to the protein. The amplitude of these fluctuations, 0.01−0.03 nm, is small and may explain why it takes milliseconds for the protein to reach its activated state (*70*), with the perturbation induced by the chromophore on the protein being relatively small. Furthermore, the β-ionone ring moves closer to helix V and away from helix VI by a distance of 0.01−0.02 nm. The amplitude of this displacement is rather small and simply means that the contact between the β-ionone ring and helix V is reinforced in the first nanoseconds of the MDs describing the isomerization of retinal. It might result either from the extension of the retinal polyene tail or from the modest increase of the vibrational level near the ring.

In this model, not all of the parts of the retinal are affected by the isomerization. The most striking example is the salt bridge between the protonated Schiff base and Glu113, an important part of the molecule, that does not seem to be affected at all in the early stage of the isomerization, because both the average distance between the two groups and the fluctuation around the average are changed by less than 0.01 nm upon activation (Figure 11A). This is in agreement with experimental data because the salt bridge between the chromophore and Glu113 is not expected to break before metarhodopsin I (∼1 ms after isomerization) (*35*).

Protein Conformational Change. At this stage, it is difficult to identify alterations in the conformation of the

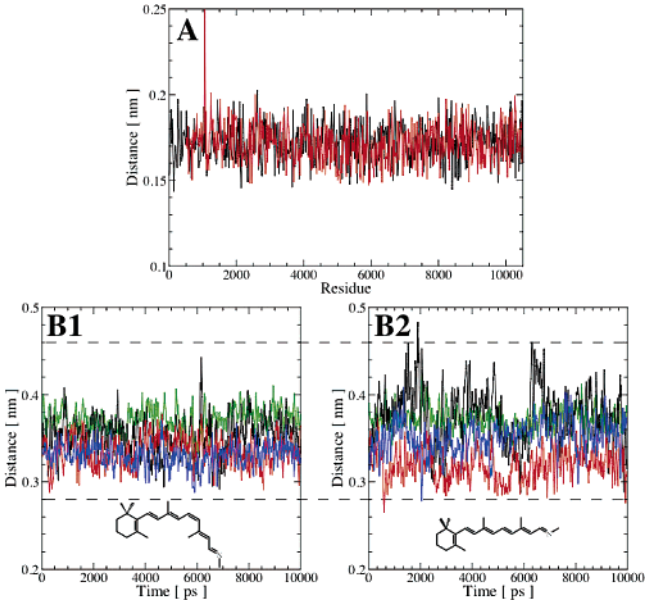

FIGURE 11: (A) Illustration of the stability of the interaction between the protonated Schiff base and the counterion (Glu113), both in the dark-adapted state (black; average = 0.172 ± 0.012 nm) and in the early stage of the activation (red; average = 0.172 ± 0.014 nm). (B1) Distance between β-ionone ring and selected residues from the binding pocket (carbon−carbon distance only): M207−ring (green; average = 0.372 ± 0.024 nm), F208−ring (black; average = 0.352 ± 0.039 nm), F212−ring (red; average = 0.336 ± 0.030 nm), and W265−ring (blue; average = 0.330 ± 0.027 nm). The increased fluctuation in these distances upon isomerization (B2) illustrates the increased level of vibration of the ring after isomerization (left, dark-adapted state; right, after isomerization): M207−ring (green; average = 0.372 ± 0.026 nm), F208−ring (black; average = 0.373 ± 0.064 nm), F212−ring (red; average = 0.322 ± 0.034 nm), and W265−ring (blue; average = 0.350 ± 0.040 nm).

protein that would arise from photoisomerization of retinal. The RMSD and RMSF plots point at various small alterations in the conformation of the protein during the MD simulations after initiation of the isomerization. Nevertheless, these changes, which can account for changes in the tilt angles of the TM helices by a few degrees (data not shown) are difficult to interpret, because they are not consistently observed along the three simulations and not very different from the fluctuations observed for MD simulations in the dark-adapted state. Longer simulation with a time scale of a few 100 ns would be required to investigate these conformational changes more thoroughly.

Simulating All-trans-retinal in the Early Stages of the Activation of Rhodopsin. In the metarhodopsin I state, the C10−C20 distance increases by more than 0.13 nm upon activation, whereas the C11−C20 remains almost unchanged (*64*). In the same photointermediate, the distance measured by rotational resonance (*52*) and the observation of ^{13}C chemical shift introduced into the β-ionone ring (*52*) (at the C16, C17, and C18 methyl groups) and into the adjoining segment of the polyene chain (at C8) suggest that the orientation of the ring remains unchanged upon isomerization. The only significant chemical-shift change that could be detected for the ring methyl groups on photoactivation was in the C18 resonance, which increased from 22.1 to 22.5 ppm (*52*). The large splitting between C16 and C17 (−4.3 ppm) describes the unique orientation of these geminal methyl groups in rhodopsin (*51*), and its retention on photoactivation is important for the determination of the mechanism of activation (*52*).

The comparison between computed and measured distances was not straightforward because, on average, an evolution of a few milliseconds is required for the chromophore to reach metarhodopsin I after isomerization. However, these values constitute a valuable point of comparison for the distorted all-*trans*-retinal simulated in the early stage after isomerization and highlight two points. First, the C11−C20 distance is very close to the value measured in the metarhodopsin I, as a result of the rotation of the C20 methyl group following the isomerization. Second, the agreement with the interatomic distances measured near the ring is less striking, mainly because of the 0.02−0.03 nm deviation from the C8−C18 distance as measured by NMR. The fluctuations result directly from the isomerization of the retinal and the stress that it induces on the chromophore and are likely to persist until the binding pocket has accommodated the all-*trans*-retinal (i.e., lumirhodopsin).

The slight increase of the C8−C18 distance was also accompanied by ring fluctuations, resulting in transient reorientation of methyl C18 away from Trp265. While the ring oscillates between its initial orientation and its new orientation, where methyl C18 is rotated away from Trp265, it cannot be interpreted as the β-ionone ring moving away from the binding pocket, as shown in Figure 11, where the average distance between the ring and the aromatic binding pocket remains constant. Only the standard deviations increase. The amplitude of the fluctuation seems too small to prevent the ring from recovering its initial orientation later once the retinal has relaxed.

Mechanism of Activation. In this present theoretical study, it is suggested that the early stages of the activation of rhodopsin are localized mainly on retinal, where a series of conformational changes occur in a sequential manner, spreading away from the isomerized bond (Figure 9B). First, the isomerization of the C11═C12 bond occurs within a few hundred femtoseconds. A recent hybrid quantum mechanical/molecular mechanical approach revealed significant rmsd increases for the polyene chain in the first 300 fs, with which our study agrees. However, this study was performed in a membrane mimetic (octanol in water) rather than in a lipid bilayer (*60*).

The rotation of methyl group C20 relative to Trp265 was observed within 1−2 ps (Figure 9B). These highly localized changes are then followed by increased fluctuations at the level of the whole retinal, mainly localized on the methyl groups and the β-ionone ring. These fluctuations, largely localized on the methyl groups and the β-ionone ring, disturb the orientation of the ring and its position relative to helix V and VI (Table 6), as well with the surrounding aromatic residues (Figure 11). The amplitude of these changes is tenuous and involves changes in the ring that are in terms of a few hundredths of nanometers and cannot be interpreted as the ring moving away from the aromatic binding pocket.

The data here suggests that the 11-*cis* bond relaxes quickly after isomerization (C11 and C12 are slightly less mobile after isomerization according to RMSF, Figure 6), transferring the mechanical stress to another part of the retinal in a sequential way, starting at the 11-*cis* bond and spreading away from the epicenter of the isomerization. The simulations suggest that the β-ionone ring plays an important role in the

Table 6: Distance between the β-Ionone Ring and Neighbor Helices[a]

	dark-adapted state	after isomerization[b]
ring−helix V (nm)	0.322 ± 0.026	0.312 ± 0.028 0.311 ± 0.026 0.317 ± 0.029
ring−helix VI (nm)	0.293 ± 0.021	0.308 ± 0.028 0.318 ± 0.032 0.308 ± 0.029

[a] Within 10 ns after isomerization, the β-ionone ring only shows a slight move toward helix V, away from helix VI. [b] Averages of a set of three MDs of the same duration.

change of the protein state through the increased fluctuations in its orientation compared to the dark-adapted state and the slight increase of the contact made with helix V (aligned with the polyene chain). Recently, helix V has been suggested to play an important role in the activation of rhodopsin (*53*). The simulations seem to show the increased interactions between retinal and helix V as part of a mechanism through which the retinal transfers the signal to the protein. The salt bridge with Glu113 at the other extreme of the chromophore anchors the ring solidly to helix III, at least during the first 10 ns of the activation (Figure 11). As a consequence, the only part of the retinal allowed to move is its ring, which also reflects a slightly less tight packing [it is known that various retinal conformers can be docked in this part of the binding pocket (*48*, *71*)].

The 10-ns MDs suggest that the small fluctuations of the ring could play a part in the process initiating the activation of the receptor. Linked with the fact the ring is still be located at the same location in metarhodopsin I (*52*), it would suggest that the small oscillations of the ring, which might be repeated over several hundred nanoseconds, could be enough to trigger the activation of the protein. This view is based on recent advances in the description of noncovalent interactions (mainly driven by atomic-force microscopy), where such interactions are described as having limited lifetimes and could fail under any level of force if applied for the right length of time (*72*). Consequently, the role of retinal would be to apply a localized perturbation at the right amplitude and time scale to initiate the protein activation.

In such a model, retinal does not need to move away from its binding pocket to achieve its activating task. The model would be compatible with both the findings that the orientation of the ring is unchanged in the metarhodopsin I (*52*) and the motions of the chromophore within the binding pocket as interpreted from the comparison of distance restraints between the chromophore and selectively labeled residues between the dark-adapted state and metarhodopsin II (*53*).

The recent NMR study of metarhodopsin II (*53*) suggests that the retinal isomerization would disrupt helix interactions locking the receptor off in the dark state and propose a mechanism of activation for rhodopsin, highlighting two essential aspects of the isomerization trajectory suggested from the retinal−protein contacts observed in the active metarhodopsin II intermediate. Those aspects include a large rotation of the C20 methyl group ($\geq 90°$) toward extracellular loop 2 and a 0.4−0.5 nm translation of the retinal chromophore toward TM helix V. The MD simulations performed here are compatible with this model and are precise when these changes take place. The results show that C20 moves away from the cytoplasmic face and rotates clockwise when looking down the polyene from Trp265 toward the β-ionone ring. From the MD model, the rotation of the C20 methyl group would happen in the first picoseconds, probably a distinctive feature of metarhodopsin, while the progressive extension of the retinal changes during the first 10 ns ($\sim$0.13 nm) suggests that much more time is required for the motion of the chromophore, interpreted as a 0.4−0.5 nm translation toward helix V. From the simulations, further extension of the retinal and translation motions of the polyene tail toward the position helix V in the dark-adapted state requires motions of helices V and VI (either translation or a change in their orientations), to generate space for the chromophore to move.

Ring Flip. In this MD study, the β-ionone ring remained in the binding-pocket over the time scale explored, in a conformation very similar to the one observed in the dark-adapted state in agreement with a recent NMR structural study on bovine rhodopsin [dark-adapted state (*51*)]. It should be noted that because of the length of the simulations, a ring flip at a longer time cannot be ruled out solely on the basis of the MD results.

The flip of the ring upon activation proposed in a previous MD simulation study (*43*) was not observed with the model used here for retinal. The rigidity of the ring compared to this previous study (where the rotation of the ring was observed) results from two factors: the conformation of the retinal in the dark-adapted state differs slightly, and the treatment of the dihedral angles is different (i.e., increasing the rigidity of the polyene tail by increasing the dihedral interactions on these bonds as if they were as rigid as a double bond). Clearly, the possibility for the ring to flip is governed by the choice of one parameter for the potential energy function describing the C5═C6−C7═C8 (data not shown). For the chromophore model to fit experimental information available for the orientation of the ring resulting from $^{13}C-^{13}C$ distance measurement by solid-state NMR (*51*, *52*), all of the dihedral interactions within the polyene chain of retinal were treated as double bonds, thus increasing the rigidity of the molecule and preventing the ring flip. This choice is also justified by the bond length recently determined by X-ray (*39*) and solid-state NMR (*65*), where deviations from ideal single C−C bond and double C═C bond lengths are observed, suggesting bond order to be larger than 1 for all bonds in the polyene chain (*39*, *65*). This illustrates the difficulties for simulating a system in which the electronic delocalization plays an important role.

Limitations. It is recognized that there are limitations to this computational approach, and simplifications are made in the building of the model (especially when related to electrostatic interactions). There are intrinsic limitations to MD simulations, which include the classical treatment of the system and a static attribution of the electronic charges to the nuclei. The other challenge introduced by rhodopsin for computational study is the large separation in time scales between the steps in the photocycle of the protein with respect to the current limits in computer simulations of large proteins. While it takes a few milliseconds for the protein to reach the activated state and much more time before the retinal is regenerated (*70*), the state-of-the-art computer

simulation of the large protein with an explicit solvent and membrane description is still limited to 10−100 ns (*44*). Therefore, MD is not yet able to follow the activation of the receptor from the dark-adapted state to the active species of rhodopsin, the so-called metarhodopsin II, where the binding and activation of the G-protein transducin (G_t) occurs (*73*−*75*). Rather, it is limited to the first photointermediates, where most conformational changes take place on the chromophore or its binding pocket.

CONCLUSIONS

The results presented here provide a continuation of the previous MD studies on retinal in rhodopsin (*42*, *43*) in the sense that the same method is applied with some refinement in the model for the chromophore as well as the protein conformation (protein model based on ref *38*). The conformation and the molecular description for the chromophore are based on a recent quantum study that describes most of the structural information available for the dark-adapted state (*48*). The experimental data regarding the conformation of retinal were also made available recently. Furthermore, the protein was modeled from a crystal structure with a resolution of 0.26 nm (1L9H) including functionally important water molecules and is simulated in an explicit lipid bilayer.

The retinal model proposed here is based on recent DFT calculations (*48*) that describe the dynamics of the bound chromophore and convergences to the experimental distance constraints (*51*, *52*, *64*). Extrapolation of this model to study the dynamics and conformation of the earliest photointermediates provides a reasonable model for the activation of retinal and suggests a possible path for the transfer of the signal to the protein. Clear structural features are suggested for both photorhodopsin and bathorhodopsin. It is also found that, although several slightly different routes for structural relaxation are available, all of them lead to similar conformational changes and that the order in which they take place defines a fixed pattern. Immediately after isomerization, the chromophore is forced into a highly strained configuration where the deformation is localized to the isomerized bond, with the other part of retinal being unchanged. The deformation is then transmitted further away to methyl group C20, which undergoes a large amplitude rotation, finally pointing toward the extracellular loops. The perturbation then reaches the ring, where increased vibrational fluctuations are observed upon isomerization of the 11-*cis* bond. The evolution of the chromophore in the multiple 10-ns MD simulations shows how the structurally distorted retinal relaxes toward a more planar geometry and suggests how the motion of retinal can be coupled to the protein, i.e., through slightly increased vibrational activity of the ring and a slight extension of retinal moving into closer contact with helix V. The geometric strain is mainly released through a swinging motion of a fraction of the polyene tail, resulting in the rotation of methyl group C20. The protonated Schiff-base interaction with Glu113 maintains this side of the chromophore rather fixed. Therefore, the perturbation generated upon isomerization of the 11-*cis* bond seems to be transferred from the retinal to the protein by a subtle mechanism mediated through the β-ionone ring, where its vibrational activity rather than perturbation of its location. In contrast, the repetition of the isomerization from different starting retinal conformations does not allow the identification of a clear and defined pattern for the activation of the protein, in agreement with the time scale required for the receptor activation (ms).

ACKNOWLEDGMENT

Dr. Minoru Sugihara is thanked for providing information describing the DFT-derived 11-*cis*,6-*s*-*cis*-retinal conformer published in 2002, and Dr. Paul Spooner is thanked for many discussions. Prof. Peter Tieleman is thanked for making available pre-equilibrated POPC bilayer. The Bionanotechnology IRC is acknowledged for consumables and computing support (through the OSC).

SUPPORTING INFORMATION AVAILABLE

By convention, all of the figures illustrating the isomerization of retinal start with the arbitrary time 0 ns, corresponding to when the illumination takes place (and where the isomerization is started). This means the time frame is independent from the amount of time the protein was previously simulated in the dark-adapted state. The advantage of this choice is to allow a direct comparison between simulations where retinal is isomerized. Note that this convention was not followed for the figures intending to show a comparison between the protein in the dark-adapted state and after isomerization (e.g., Figure 4). For those figures, the time frame used is the one corresponding to the simulation in the dark-adapted state, where the starting time for the simulations where retinal is isomerized is 500, 1000, and 1500 ps, respectively. Graphs of simulations with alternate starting points (retinal isomerization after 1000- or 1500-ps MD in the dark-adapted state), corresponding to Figures 3, 4, 5, 7, 9, 11 in the paper. This material is available free of charge via the Internet at http://pubs.acs.org.

REFERENCES

1. Wald, G. (1968) The molecular basis of visual excitation, *Nature 219*, 800−807.
2. Sakmar, T. P. (1998) Rhodopsin: A prototypical G protein-coupled receptor, *Prog. Nucleic Acid Res. Mol. Biol. 59*, 1−34.
3. Okada, T., Ernst, O. P., Palczewski, K., and Hofmann, K. P. (2001) Activation of rhodopsin: New insights from structural and biochemical studies, *Trends Biochem. Sci. 26*, 318−324.
4. Sakmar, T. P., Menon, S. T., Marin, E. P., and Awad, E. S. (2002) Rhodopsin: Insights from recent structural studies, *Annu. Rev. Biophys. Biomol. Struct. 31*, 443−484.
5. Burns, M. E., and Baylor, D. A. (2001) Activation, deactivation, and adaptation in vertebrate photoreceptor cells, *Annu. Rev. Neurosci. 24*, 779−805.
6. Hubbell, W. L., Altenbach, C., Hubbell, C. M., and Khorana, H. G. (2003) Rhodopsin structure, dynamics, and activation: A perspective from crystallography, site-directed spin labeling, sulfhydryl reactivity, and disulfide cross-linking, *Adv. Protein Chem. 63*, 243−290.
7. Albert, A. D., and Yeagle, P. L. (2002) Structural studies on rhodopsin, *Biochim. Biophys. Acta 1565*, 183−195.
8. Birge, R. R., Einterz, C. M., Knapp, H. M., and Murray, L. P. (1988) The nature of the primary photochemical events in rhodopsin and isorhodopsin, *Biophys. J. 53*, 367−385.
9. Shichida, Y., and Imai, H. (1998) Visual pigment: G-protein-coupled receptor for light signals, *Cell Mol. Life Sci. 54*, 1299−1315.
10. Kliger, D. S., and Lewis, J. W. (1995) Spectral and kinetic characterization of visual pigment photointermediates, *Isr. J. Chem. 35*, 289−307.
11. Pan, D., and Mathies, R. A. (2001) Chromophore structure in lumirhodopsin and metarhodopsin I by time-resolved resonance Raman microchip spectroscopy, *Biochemistry 40*, 7929−7936.

12. Kandori, H., Shichida, Y., and Yoshizawa, T. (2001) Photoisomerization in rhodopsin, *Biochemistry (Moscow) 66*, 1197−1209.
13. Schoenlein, R. W., Peteanu, L. A., Mathies, R. A., and Shank, C. V. (1991) The first step in vision: Femtosecond isomerization of rhodopsin, *Science 254*, 412−415.
14. Kandori, H., Shichida, Y., and Yoshizawa, T. (1989) Absolute absorption spectra of batho- and photorhodopsins at room temperature. Picosecond laser photolysis of rhodopsin in polyacrylamide, *Biophys. J. 56*, 453−457.
15. Mathies, R. A. (1999) Photons, femtoseconds, and dipolar interactions: A molecular picture of the primary events in vision, *Novartis Found. Symp. 224*, 70−84, discussion 84−101.
16. Shieh, T., Han, M., Sakmar, T. P., and Smith, S. O. (1997) The steric trigger in rhodopsin activation, *J. Mol. Biol. 269*, 373−384.
17. Palings, I., van den Berg, E. M., Lugtenburg, J., and Mathies, R. A. (1989) Complete assignment of the hydrogen out-of-plane wagging vibrations of bathorhodopsin: Chromophore structure and energy storage in the primary photoproduct of vision, *Biochemistry 28*, 1498−1507.
18. Cooper, A. (1979) Energy uptake in the first step of visual excitation, *Nature 282*, 531−533.
19. Honig, B., Ebrey, T., Callender, R. H., Dinur, U., and Ottolenghi, M. (1979) Photoisomerization, energy storage, and charge separation: A model for light energy transduction in visual pigments and bacteriorhodopsin, *Proc. Natl. Acad. Sci. U.S.A. 76*, 2503−2507.
20. de Grip, W. J., Gray, D., Gillespie, J., Bovee, P. H., van den Berg, E. M., Lugtenburg, J., and Rothschild, K. J. (1988) Photoexcitation of rhodopsin: Conformation changes in the chromophore, protein, and associated lipids as determined by FTIR difference spectroscopy, *Photochem. Photobiol. 48*, 497−504.
21. Eyring, G., and Mathies, R. (1979) Resonance Raman studies of bathorhodopsin: Evidence for a protonated Schiff base linkage, *Proc. Natl. Acad. Sci. U.S.A. 76*, 33−37.
22. Bagley, K. A., Balogh-Nair, V., Croteau, A. A., Dollinger, G., Ebrey, T. G., Eisenstein, L., Hong, M. K., Nakanishi, K., and Vittitow, J. (1985) Fourier transform infrared difference spectroscopy of rhodopsin and its photoproducts at low temperature, *Biochemistry 24*, 6055−6071.
23. Deng, H., and Callender, R. H. (1987) A study of the Schiff base mode in bovine rhodopsin and bathorhodopsin, *Biochemistry 26*, 7418−7426.
24. Smith, S. O., Courtin, J., de Groot, H., Gebhard, R., and Lugtenburg, J. (1991) ^{13}C magic-angle spinning NMR studies of bathorhodopsin, the primary photoproduct of rhodopsin, *Biochemistry 30*, 7409−7415.
25. Popp, A., Ujj, L., and Atkinson, G. H. (1996) Bathorhodopsin structure in the room-temperature rhodopsin photosequence: Picosecond time-resolved coherent anti-Stokes Raman scattering, *Proc. Natl. Acad. Sci. U.S.A. 93*, 372−376.
26. Marcus, M. A., and Lewis, A. (1979) Assigning the resonance Raman spectral features of rhodopsin, isorhodopsin, and bathorhodopsin in bovine photostationary state spectra, *Photochem. Photobiol. 29*, 699−702.
27. Jager, S., Lewis, J. W., Zvyaga, T. A., Szundi, I., Sakmar, T. P., and Kliger, D. S. (1997) Chromophore structural changes in rhodopsin from nanoseconds to microseconds following pigment photolysis, *Proc. Natl. Acad. Sci. U.S.A. 94*, 8557−8562.
28. Hug, S. J., Lewis, J. W., Einterz, C. M., Thorgeirsson, T. E., and Kliger, D. S. (1990) Nanosecond photolysis of rhodopsin: Evidence for a new, blue-shifted intermediate, *Biochemistry 29*, 1475−1485.
29. Lewis, J. W., Fan, G. B., Sheves, M., Szundi, I., and Kliger, D. S. (2001) Steric barrier to bathorhodopsin decay in 5-demethyl and mesityl analogues of rhodopsin, *J. Am. Chem. Soc. 123*, 10024−10029.
30. Lewis, J. W., Pinkas, M., Sheves, M., Ottolenghi, M., and Kliger, D. S. (1995) Structural changes in early photolysis intermediates of rhodopsin from time-resolved spectral measurements of artificial pigments sterically hindered along the chromophores chain, *J. Am. Chem. Soc. 117*, 918−923.
31. Randall, C. E., Lewis, J. W., Hug, S. J., Björling, S. C., Eisner-Shanas, I., Friedman, I., Ottolenghi, M., Sheves, M., and Kliger, D. S. (1991) A new photolysis intermediate in artificial and native visual pigments, *J. Am. Chem. Soc. 113*, 3473−3485.
32. Cohen, G. B., Oprian, D. D., and Robinson, P. R. (1992) Mechanism of activation and inactivation of opsin: Role of Glu113 and Lys296, *Biochemistry 31*, 12592−12601.
33. Kuwata, O., Yuan, C., Misra, S., Govindjee, R., and Ebrey, T. G. (2001) Kinetics and pH dependence of light-induced deprotonation of the Schiff base of rhodopsin: Possible coupling to proton uptake and formation of the active form of Meta II, *Biochemistry (Moscow) 66*, 1283−1299.
34. Smith, S. O., de Groot, H., Gebhard, R., and Lugtenburg, J. (1992) Magic angle spinning NMR studies on the metarhodopsin II intermediate of bovine rhodopsin: Evidence for an unprotonated Schiff base, *Photochem. Photobiol. 56*, 1035−1039.
35. Yan, E. C., Kazmi, M. A., Ganim, Z., Hou, J. M., Pan, D., Chang, B. S., Sakmar, T. P., and Mathies, R. A. (2003) Retinal counterion switch in the photoactivation of the G protein-coupled receptor rhodopsin, *Proc. Natl. Acad. Sci. U.S.A. 100*, 9262−9267.
36. Palczewski, K., Kumasaka, T., Hori, T., Behnke, C. A., Motoshima, H., Fox, B. A., Le Trong, I., Teller, D. C., Okada, T., Stenkamp, R. E., Yamamoto, M., and Miyano, M. (2000) Crystal structure of rhodopsin: A G protein-coupled receptor, *Science 277*, 687−690.
37. Okada, T., and Palczewski, K. (2001) Crystal structure of rhodopsin: Implications for vision and beyond, *Curr. Opin. Struct. Biol. 11*, 420−426.
38. Okada, T., Fujiyoshi, Y., Silow, M., Navarro, J., Landau, E. M., and Shichida, Y. (2002) Functional role of internal water molecules in rhodopsin revealed by X-ray crystallography, *Proc. Natl. Acad. Sci. U.S.A. 99*, 5982−5987.
39. Okada, T., Sugihara, M., Bondar, A. N., Elstner, M., Entel, P., and Buss, V. (2004) The retinal conformation and its environment in rhodopsin in light of a new 2.2 Å crystal structure, *J. Mol. Biol. 342*, 571−583.
40. Li, J., Edwards, P. C., Burghammer, M., Villa, C., and Schertler, G. F. (2004) Structure of bovine rhodopsin in a trigonal crystal form, *J. Mol. Biol.*, in press.
41. Choi, G., Landin, J., Galan, J. F., Birge, R. R., Albert, A. D., and Yeagle, P. L. (2002) Structural studies of metarhodopsin II, the activated form of the G-protein coupled receptor, rhodopsin, *Biochemistry 41*, 7318−7324.
42. Röhrig, U. F., Guidoni, L., and Rothlisberger, U. (2002) Early steps of the intramolecular signal transduction in rhodopsin explored by molecular dynamics simulations, *Biochemistry 41*, 10799−10809.
43. Saam, J., Tajkhorshid, E., Hayashi, S., and Schulten, K. (2002) Molecular dynamics investigation of primary photoinduced events in the activation of rhodopsin, *Biophys. J. 83*, 3097−3112.
44. Crozier, P. S., Stevens, M. J., Forrest, L. R., and Woolf, T. B. (2003) Molecular dynamics simulation of dark-adapted rhodopsin in an explicit membrane bilayer: Coupling between local retinal and larger scale conformational change, *J. Mol. Biol. 333*, 493−514.
45. Huber, T., Botelho, A. V., Beyer, K., and Brown, M. F. (2004) Membrane model for the G-protein-coupled receptor rhodopsin: Hydrophobic interface and dynamical structure, *Biophys. J. 86*, 2078−2100.
46. Yamada, A., Kakitani, T., Yamamoto, S., and Yamamoto, T. (2002) A computational study on the stability of the protonated Schiff base of retinal in rhodopsin, *Chem. Phys. Lett. 366*, 670−675.
47. Buss, V., Sugihara, M., Entel, P., and Hafner, J. (2003) Thr94 and Wat2b effect protonation of the retinal chromophore in rhodopsin, *Angew. Chem. Int. Ed. 42*, 3245−3247.
48. Sugihara, M., Buss, V., Entel, P., Elstner, M., and Frauenheim, T. (2002) 11-*cis*-retinal protonated Schiff base: Influence of the protein environment on the geometry of the rhodopsin chromophore, *Biochemistry 41*, 15259−15266.
49. Sugihara, M., Buss, V., Entel, P., and Hafner, J. (2004) The nature of the complex counterion of the chromophore in rhodopsin, *J. Phys. Chem. B 108*, 3673−3680.
50. Verdegem, P. J. E., Helmle, M., Lugtenburg, J., and de Groot, H. J. M. (1997) Internuclear distance measurements up to 0.44 nm for retinals in the solid state with 1-D rotational resonance ^{13}C MAS NMR spectroscopy, *J. Am. Chem. Soc. 119*, 169−174.
51. Spooner, P. J., Sharples, J. M., Verhoeven, M. A., Lugtenburg, J., Glaubitz, C., and Watts, A. (2002) Relative orientation between the β-ionone ring and the polyene chain for the chromophore of rhodopsin in native membranes, *Biochemistry 41*, 7549−7555.
52. Spooner, P. J., Sharples, J. M., Goodall, S. C., Seedorf, H., Verhoeven, M. A., Lugtenburg, J., Bovee-Geurts, P. H., de Grip, W. J., and Watts, A. (2003) Conformational similarities in the β-ionone ring region of the rhodopsin chromophore in its ground

state and after photoactivation to the metarhodopsin-I intermediate, *Biochemistry 42*, 13371−13378.
53. Patel, A. B., Crocker, E., Eilers, M., Hirshfeld, A., Sheves, M., and Smith, S. O. (2004) Coupling of retinal isomerization to the activation of rhodopsin, *Proc. Natl. Acad. Sci. U.S.A. 101*, 10048−10053.
54. Smith, S. O., Palings, I., Copie, V., Raleigh, D. P., Courtin, J., Pardoen, J. A., Lugtenburg, J., Mathies, R. A., and Griffin, R. G. (1987) Low-temperature solid-state ^{13}C NMR studies of the retinal chromophore in rhodopsin, *Biochemistry 26*, 1606−1611.
55. Mollevanger, L. C., Kentgens, A. P., Pardoen, J. A., Courtin, J. M., Veeman, W. S., Lugtenburg, J., and de Grip, W. J. (1987) High-resolution solid-state ^{13}C NMR study of carbons C-5 and C-12 of the chromophore of bovine rhodopsin. Evidence for a 6-*s*-*cis* conformation with negative-charge perturbation near C-12, *Eur. J. Biochem. 163*, 9−14.
56. Smith, S. O., Palings, I., Miley, M. E., Courtin, J., de Groot, H., Lugtenburg, J., Mathies, R. A., and Griffin, R. G. (1990) Solid-state NMR studies of the mechanism of the opsin shift in the visual pigment rhodopsin, *Biochemistry 29*, 8158−8164.
57. Verhoeven, M. A., Creemers, A. F., Bovee-Geurts, P. H., de Grip, W. J., Lugtenburg, J., and de Groot, H. J. (2001) Ultra-high-field MAS NMR assay of a multispin labeled ligand bound to its G-protein receptor target in the natural membrane environment: Electronic structure of the retinylidene chromophore in rhodopsin, *Biochemistry 40*, 3282−3288.
58. Creemers, A. F., Kiihne, S., Bovee-Geurts, P. H., de Grip, W. J., Lugtenburg, J., and de Groot, H. J. (2002) ^{1}H and ^{13}C MAS NMR evidence for pronounced ligand−protein interactions involving the ionone ring of the retinylidene chromophore in rhodopsin, *Proc. Natl. Acad. Sci. U.S.A. 99*, 9101−9106.
59. Teller, D. C., Okada, T., Behnke, C. A., Palczewski, K., and Stenkamp, R. E. (2001) Advances in determination of a high-resolution three-dimensional structure of rhodopsin, a model of G-protein-coupled receptors (GPCRs), *Biochemistry 40*, 7761−7772.
60. Röhrig, U. F., Guidoni, L., Laio, A., Frank, I., and Rothlisberger, U. (2004) A molecular spring for vision, *J. Am. Chem. Soc. 126*, 15328−15329.
61. Berger, O., Edholm, O., and Jahnig, F. (1997) Molecular dynamics simulations of a fluid bilayer of dipalmitoylphosphatidylcholine at full hydration, constant pressure, and constant temperature, *Biophys. J. 72*, 2002−2013.
62. Berendsen, H. J. C., Griegera, J. R., and Straatsma, T. P. (1987) The missing term in effective pair potentials, *J. Phys. Chem. 91*, 6269−6271.
63. Sali, A., Potterton, L., Yuan, F., van Vlijmen, H., and Karplus, M. (1995) Evaluation of comparative protein modeling by MODELLER, *Proteins 23*, 318−326.
64. Verdegem, P. J., Bovee-Geurts, P. H., de Grip, W. J., Lugtenburg, J., and de Groot, H. J. (1999) Retinylidene ligand structure in bovine rhodopsin, metarhodopsin-I, and 10-methylrhodopsin from internuclear distance measurements using ^{13}C-labeling and 1-D rotational resonance MAS NMR, *Biochemistry 38*, 11316−11324.
65. Carravetta, M., Zhao, X., Johannessen, O. G., Lai, W. C., Verhoeven, M. A., Bovee-Geurts, P. H., Verdegem, P. J., Kiihne, S., Luthman, H., de Groot, H. J., de Grip, W. J., Lugtenburg, J., and Levitt, M. H. (2004) Protein-induced bonding perturbation of the rhodopsin chromophore detected by double-quantum solid-state NMR, *J. Am. Chem. Soc. 126*, 3948−3953.
66. Buss, V. (2001) Inherent chirality of the retinal chromophore in rhodopsin−A nonempirical theoretical analysis of chiroptical data, *Chirality 13*, 13−23.
67. Faraldo-Gomez, J. D., Smith, G. R., and Sansom, M. S. (2002) Setting up and optimization of membrane protein simulations, *Eur. Biophys. J. 31*, 217−227.
68. Humphrey, W., Dalke, A., and Schulten, K. (1996) VMD: Visual molecular dynamics, *J. Mol. Graphics 14*, 33−38, 27−38.
69. Hayashi, S., Tajkhorshid, E., and Schulten, K. (2002) Structural changes during the formation of early intermediates in the bacteriorhodopsin photocycle, *Biophys. J. 83*, 1281−1297.
70. Klein-Seetharaman, J. (2002) Dynamics in rhodopsin, *ChemBioChem 3*, 981−986.
71. Singh, D., Hudson, B. S., Middleton, C., and Birge, R. R. (2001) Conformation and orientation of the retinyl chromophore in rhodopsin: A critical evaluation of recent NMR data on the basis of theoretical calculations results in a minimum energy structure consistent with all experimental data, *Biochemistry 40*, 4201−4204.
72. Evans, E. (1998) Energy landscapes of biomolecular adhesion and receptor anchoring at interfaces explored with dynamic force spectroscopy, *Faraday Discuss.*, 1−16.
73. Fain, G. L., Matthews, H. R., Cornwall, M. C., and Koutalos, Y. (2001) Adaptation in vertebrate photoreceptors, *Physiol. Rev. 81*, 117−151.
74. Hamm, H. E. (2001) How activated receptors couple to G proteins, *Proc. Natl. Acad. Sci. U.S.A. 98*, 4819−4821.
75. Polans, A., Baehr, W., and Palczewski, K. (1996) Turned on by Ca^{2+}! The physiology and pathology of Ca^{2+}-binding proteins in the retina, *Trends Neurosci. 19*, 547−554.
76. Feng, X., Verdegem, P. J., Lee, Y. K., Sandström, D., Edén, M., Bonvee-Geurts, P., de Grip, W. J., Lugtenburg, J., de Groot, H. J. M., and Levitt, M. H. (1997) Direct determination of a molecular torsional angle in the membrane protein rhodopsin by solid-state NMR, *J. Am. Chem. Soc. 119*, 6853−6857.
77. de Grip, W. J., DeLange, F., Klaassen, C. H., Verdegem, P. J., Wallace-Williams, S., Creemers, A. F., Bergo, V., Bovee, P. H., Raap, J., Rothschild, K. J., de Groot, H. J., and Lugtenburg, J. (1999) Photoactivation of rhodopsin: Interplay between protein and chromophore, *Novartis Found. Symp. 224*, 102−118, discussion 118−123.

BI0506019